Catalytic Role for Arginine 188 in the C−C Hydrolase Catalytic Mechanism for *Escherichia coli* MhpC and *Burkholderia xenovorans* LB400 BphD†

Chen Li,‡ Jian-Jun Li,‡ Mark G. Montgomery,§ Stephen P. Wood,§ and Timothy D. H. Bugg*,‡

Department of Chemistry, University of Warwick, Coventry CV4 7AL, U.K., and School of Biological Sciences, University of Southampton, Bassett Crescent East, Southampton SO16 7PX, U.K.

Received June 23, 2006; Revised Manuscript Received August 15, 2006

ABSTRACT: The α/β-hydrolase superfamily, comprised mainly of esterase and lipase enzymes, contains a family of bacterial C−C hydrolases, including MhpC and BphD which catalyze the hydrolytic C−C cleavage of *meta*-ring fission intermediates on the *Escherichia coli* phenylpropionic acid pathway and *Burkholderia xenovorans* LB400 biphenyl degradation pathway, respectively. Five active site amino acid residues (Arg-188, Asn-109, Phe-173, Cys-261, and Trp-264) were identified from sequence alignments that are conserved in C−C hydrolases, but not in enzymes of different function. Replacement of Arg-188 in MhpC with Gln and Lys led to 200- and 40-fold decreases, respectively, in k_{cat}; the same replacements for Arg-190 of BphD led to 400- and 700-fold decreases, respectively, in k_{cat}. Pre-steady-state kinetic analysis of the R188Q MhpC mutant revealed that the first step of the reaction, keto−enol tautomerization, had become rate-limiting, indicating that Arg-188 has a catalytic role in ketonization of the dienol substrate, which we propose is via substrate destabilization. Mutation of nearby residues Phe-173 and Trp-264 to Gly gave 4−10-fold reductions in k_{cat} but 10−20-fold increases in K_m, indicating that these residues are primarily involved in substrate binding. The X-ray structure of a succinate−H263A MhpC complex shows concerted movements in the positions of both Phe-173 and Trp-264 that line the approach to Arg-188. Mutation of Asn-109 to Ala and His yielded 200- and 350-fold reductions, respectively, in k_{cat} and pre-steady-state kinetic behavior similar to that of a previous S110A mutant, indicating a role for Asn-109 is positioning the active site loop containing Ser-110. The catalytic role of Arg-188 is rationalized by a hydrogen bond network close to the C-1 carboxylate of the substrate, which positions the substrate and promotes substrate ketonization, probably via destabilization of the bound substrate.

The α/β-hydrolase enzyme superfamily, first identified in 1992 (*1*), contains enzymes of diverse hydrolytic function but sharing a similar structural fold, consisting of an eight-stranded β-sheet, with α-helices or an additional small domain between each pair of parallel β-strands (*2*). Most members of the α/β-hydrolase family are esterase and lipase enzymes that catalyze ester hydrolysis reactions, using a serine-histidine-aspartic acid catalytic triad (*3*, *4*). The enzymes haloalkane dehalogenase (*5*) and epoxide hydrolase (*6*), containing an aspartic acid nucleophile in place of serine, carry out the nucleophilic attack on haloalkane and epoxide substrates, respectively, followed by hydrolysis of a covalent ester intermediate. There are also enzymes that catalyze peptide hydrolysis reactions, such as prolyl oligopeptidase (*7*).

Within the α/β-hydrolase superfamily are a family of C−C hydrolases, which catalyze the hydrolytic C−C cleavage of ring cleavage products on bacterial *meta*-cleavage pathways responsible for the degradation of aromatic compounds in soil. The catalytic triad of *Pseudomonas putida* XylF was identified as Ser-107, Asp-228, and His-256, and each of these residues was demonstrated using site-directed mutagenesis to be essential for catalytic activity (*8*). Studies in our laboratory on *Escherichia coli* MhpC,[1] a C−C hydrolase

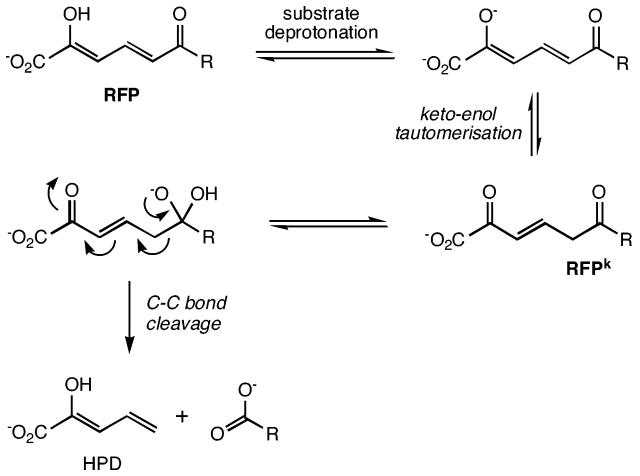

FIGURE 1: Reaction scheme showing key steps in the MhpC-catalyzed C−C bond hydrolysis. The reaction consists of an initial deprotonation of the dienol substrate, ketonization to give a keto intermediate (RFP^k), base-catalyzed attack by an active site water molecule, and C−C fragmentation to yield 2-hydroxypentadienoic acid (HPD) and acid product. R = $CH_2CH_2CO_2H$ for MhpC and Ph for BphD.

† This work was supported by BBSRC (Grant B20467), the University of Warwick, and ORS.

* To whom correspondence should be addressed. Telephone: 02476-573018. Fax: 02476-524112. E-mail: T.D.Bugg@warwick.ac.uk.

‡ University of Warwick.

§ University of Southampton.

10.1021/bi061253t CCC: $33.50
Published on Web 09/21/2006

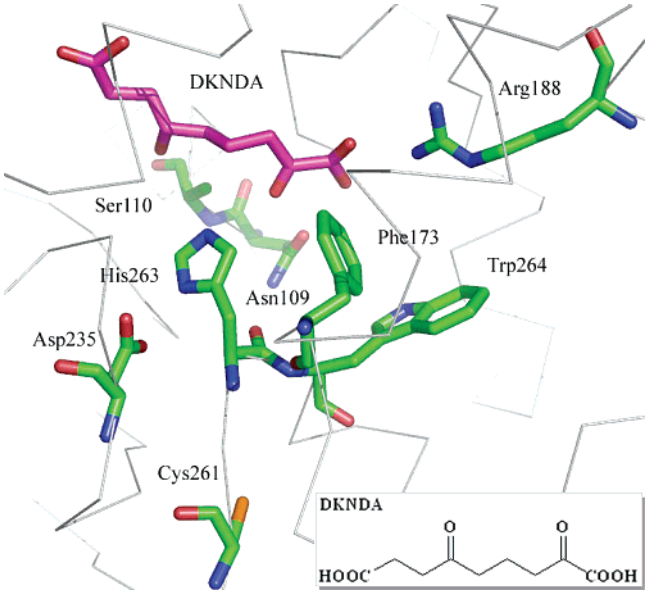

FIGURE 2: Active site of MhpC, complexed with noncleavable substrate analogue DKNDA (structure given), showing the location of active site residues Asn-109, Arg-188, Phe-173, Trp-264, and Cys-261, and the catalytic triad comprising Ser-110, His-263, and Asp-235.

on the phenylpropionic acid catabolic pathway, have shown that the reaction mechanism involves two half-reactions: an initial keto−enol tautomerization to form a discrete keto intermediate followed by a stereospecific C−C fragmentation reaction, as shown in Figure 1 (*9*, *10*). Mechanistic studies on the reactions catalyzed by *E. coli* MhpC and *Burkholderia xenovorans* LB400 have provided evidence to support a mechanism involving base-catalyzed attack of water on a keto intermediate (*11*, *12*), and in the accompanying paper (*35*), the *gem*-diol reaction intermediate has been observed directly by ^{13}C NMR spectroscopy.

The factors that control the catalysis of C−C hydrolytic cleavage in this family of enzymes, as opposed to C−O esterolytic cleavage, or catalysis of other reaction pathways, are at present unknown. In the C−C hydrolase family of sequence-related α/β-hydrolases are esterases, lipases, cofactor-independent haloperoxidases, and peptidases. Structure determination of *E. coli* MhpC complexed with a noncleavable substrate analogue (*13*) revealed that the guanidinium side chain of Arg-188 was positioned 2.6 Å from the C-1 carboxylate of the substrate and that the aromatic side chains of Phe-173 and Trp-264 are positioned close to the bound substrate analogue (see Figure 2). Amino acid sequence alignments (see below) indicated that these residues were found only in C−C hydrolase enzymes, not in esterase or haloperoxidase enzymes. This paper describes kinetic studies on site-directed mutants of Arg-188, Phe-173, Trp-264, and two other active site residues, in an effort to determine their role in C−C hydrolase catalysis, and the structure determination of a H263A mutant enzyme in which concerted movements of these residues are observed.

[1] Abbreviations: MhpC, 2-hydroxy-6-ketonona-2,4-diene-1,9-dioic acid 5,6-hydrolase; BphD, 2-hydroxy-6-keto-6-phenylhexa-2,4-dienoic acid 5,6-hydrolase; RFP, ring fission product (**1**); HPD, 2-hydroxypentadienoic acid; DKNDA, 2,6-diketonona-1,9-dioic acid; IPTG, β-isopropyl thiogalactoside; SDS−PAGE, sodium dodecyl sulfate−polyacrylamide gel electrophoresis.

MATERIALS AND METHODS

Materials. The natural substrate for MhpC was prepared enzymatically (*9*), and the natural substrate for BphD was chemically synthesized (*14*), as previously described. Wild-type MhpC was expressed and purified as previously described (*15*). All chemicals and biochemicals were purchased from Sigma-Aldrich Chemical Co. or Bio-Rad Laboratories unless stated otherwise.

Construction of Site-Directed Mutants of MhpC and BphD. All MhpC site-directed mutants and BphD R188K were constructed from the *E. coli mhpC* and *B. xenovorans* LB400 *bphD* genes using Quikchange site-directed mutagenesis kits from Stratagen as previously described (*15*). The BphD R188Q mutant was created using the overlap extension PCR-based method (*16*). Oligonucleotides were custom-synthesized by Sigma Genosys and are listed in Table 1. The mutations were confirmed by DNA sequencing, and the plasmids were used to transform *E. coli* BL21(DE3) competent cells. MhpC mutants were expressed and purified by Q-Sepharose anion exchange chromatography as previously described (*15*), giving yields of 30−50 mg of enzyme of >95% homogeneity from a 2 L culture. BphD mutants were expressed in a pET-14b vector (Novagen) as an N-terminal His_6 fusion protein and purified with a Talon column (Clontech Laboratories) as described in ref *35*, giving yields of 20−50 mg of enzyme of >95% homogeneity from a 2 L culture.

Kinetic Assays. Steady-state kinetic parameters of MhpC and BphD mutants were routinely determined at pH 8.0 and 25 °C as the decrease in absorbance at 394 nm (ϵ_{394} = 15 600 M^{-1} cm^{-1}) and 434 nm (ϵ_{434} = 26 300 M^{-1} cm^{-1}), respectively, due to the consumption of the corresponding natural substrate (*15*). A typical assay mixture of contained substrate ($^1/_5K_M \sim 5K_M$) in 1 mL of 50 mM potassium phosphate buffer (pH 8.0), to which 10 μL of enzyme was added. K_M and k_{cat} were calculated using an Eadie−Hofstee plot.

Stopped-flow assays were carried out in 50 mM potassium phosphate buffer (pH 7.0) according to the previously described procedure (*15*). In each experiment, solutions of 1 mg/mL enzyme and 33 mM substrate (1:1 [E]:[S] molar ratio) were mixed rapidly in the reaction chamber at room temperature. Disappearance of the substrate was monitored at both 394 and 317 nm for the MhpC-catalyzed reaction and at 434 and 341 nm for the BphD-catalyzed reaction. The formation of the dienol product was monitored at 270 nm. Data of each shot were recorded and simulated with single-, double-, or treble-exponential kinetic models, from which the best-fit kinetic parameters were deduced.

Determination of the Structure of the H263A MhpC Mutant. Preparation of the mutant enzyme was described previously (*15*). Crystallization conditions for the mutant enzyme were screened by hanging drop vapor diffusion. Orthorhombic crystals ($P4_32_12$, $a = b = 80.3$ Å, $c = 427.04$ Å) of the H263A mutant of MhpC grew by precipitation with 15% (w/v) PEG 4K in vapor diffusion from a succinate buffer prepared by mixing 50 mM sodium succinate (pH 3.9) and 100 mM ammonium succinate (pH 7.0) in a 1:2 ratio. Crystals were vitrified by being immersed in liquid ethane using mother liquor supplemented with 30% (v/v) glycerol as a cryoprotectant. X-ray data were collected at the ESRF

Table 1: PCR Primers for Site-Directed Mutagenesis of *mhpC* and *bphD* Genes

	Mutant	Direction	5' - **Primer Sequence** – 3'
MhpC	R188Q	forward	CCTGTTTGAAGCGCAGCTGAATAATATGCTGTCG
		reverse	CGACAGCATATTATTCAGCTGCGCTTCAAACAGG
	R188K	forward	CCTGTTTGAAGCGAAGCTGAATAATATGCTGTCG
		reverse	CGACAGCATATTATTCAGCTTCGCTTCAAACAGG
	C261A	forward	GCATATCTTCCGCGACGCTGGTCACTGGGCGCAG
		reverse	CTGCGCCCAGTGACCAGCGTCGCGGAAGATATGC
	W264G	forward	CCGCGACTGTGGTCACGGGGCGCAGTGGGAACAT
		reverse	ATGTTCCCACTGCGCCCCGTGACCACAGTCGCGG
	N109A	forward	AATCCACCTGCTGGGCGCCTCGATGGGGGGCCAT
		reverse	ATGGCCCCCCATCGAGGCGCCCAGCAGGTGGATT
	N109H	forward	AATCCACCTGCTGGGCCACTCGATGGGGGGCCAT
		reverse	ATGGCCCCCCATCGAGTGGCCCAGCAGGTGGATT
	F173G	forward	GCTGATGATGGATATCGGCGTTTTTGATACCAGC
		reverse	GCTGGTATCAAAAACGCCGATATCCATCATCAGC
	F173D	forward	GCTGATGATGGATATCGACGTTTTTGATACCAGC
		reverse	GCTGGTATCAAAAACGTCGATATCCATCATCAGC
BphD	R190Q	forward	GCTGCAGGGCCAGTGGGAAGCCATTCAGC
		reverse	TGAATGGCTTCCCACTGGCCCTGCAGCAACTC
	R190K	forward	GAGTTGCTGCAGGGCAAGTGGGAAGCCATTCAGCG
		reverse	CGCTGAATGGCTTCCCACTTGCCCTGCAGCAACTC

(Grenoble, France) on station ID23.1 ($\lambda = 1.069$ Å) with a Quantum ADSC detector at 100 K and processed with MOSFILM and programs of the CCP4 suite (*17*, *18*). The data extended to 2.0 Å resolution. Molecular replacement was performed with MOLREP (*19*) and the structure refined with CNS (*20*). Following initial rigid body refinement and positional refinements with tight NCS restraints, these were relaxed as the model improved and water molecules were added. Individual *B*-factors were refined. Some side chains (W264 and F173) were clearly present in different conformations in different subunits and refined well with dual occupancy in these alternate positions, producing flat difference maps. Model building was carried out using QUANTA (*21*), and diagrams were generated with PYMOL (*22*).

RESULTS

Identification of Amino Acid Residues Specific to C−C Hydrolase Function. Alignment of the amino acid sequences of *E. coli* MhpC and *B. xenovorans* BphD with the sequences of esterases and haloperoxidases in this family of α/β-hydrolases was carried out using CLUSTAL (*23*). The alignment is shown in Figure 3. A search was made for residues that were conserved in C−C hydrolase enzymes MhpC, BphD, XylF, and DmpD but not conserved in enzymes of different function, which might be key determinants in C−C hydrolase catalysis. The following residues were found: Asn-109, Phe-173, Arg-188, Cys-261, and Trp-264. In related esterase and haloperoxidase sequences, Asn-109 is found as either histidine or phenylalanine; Phe-173, Arg-188, and Trp-264 are always substituted with an aspartate, a serine, or a glycine residue, respectively. The position corresponding to Cys-261 in MhpC is occupied by hydrophobic residues, such as Phe, Ala, and Leu.

The location of each of these residues is shown in Figure 2. Phe-173 and Arg-188 are both found in the "lid" domain of MhpC, a domain comprised of four α-helices that lies over the active site, connected via a flexible hinge domain. The guanidinium side chain of Arg-188 extends into the active site and is positioned 2.6 Å from the C-1 carboxylate of the bound substrate analogue, suggesting that may be involved in substrate binding. The aryl side chain of Phe-173 is positioned 3.9 Å from the substrate, close to the indole

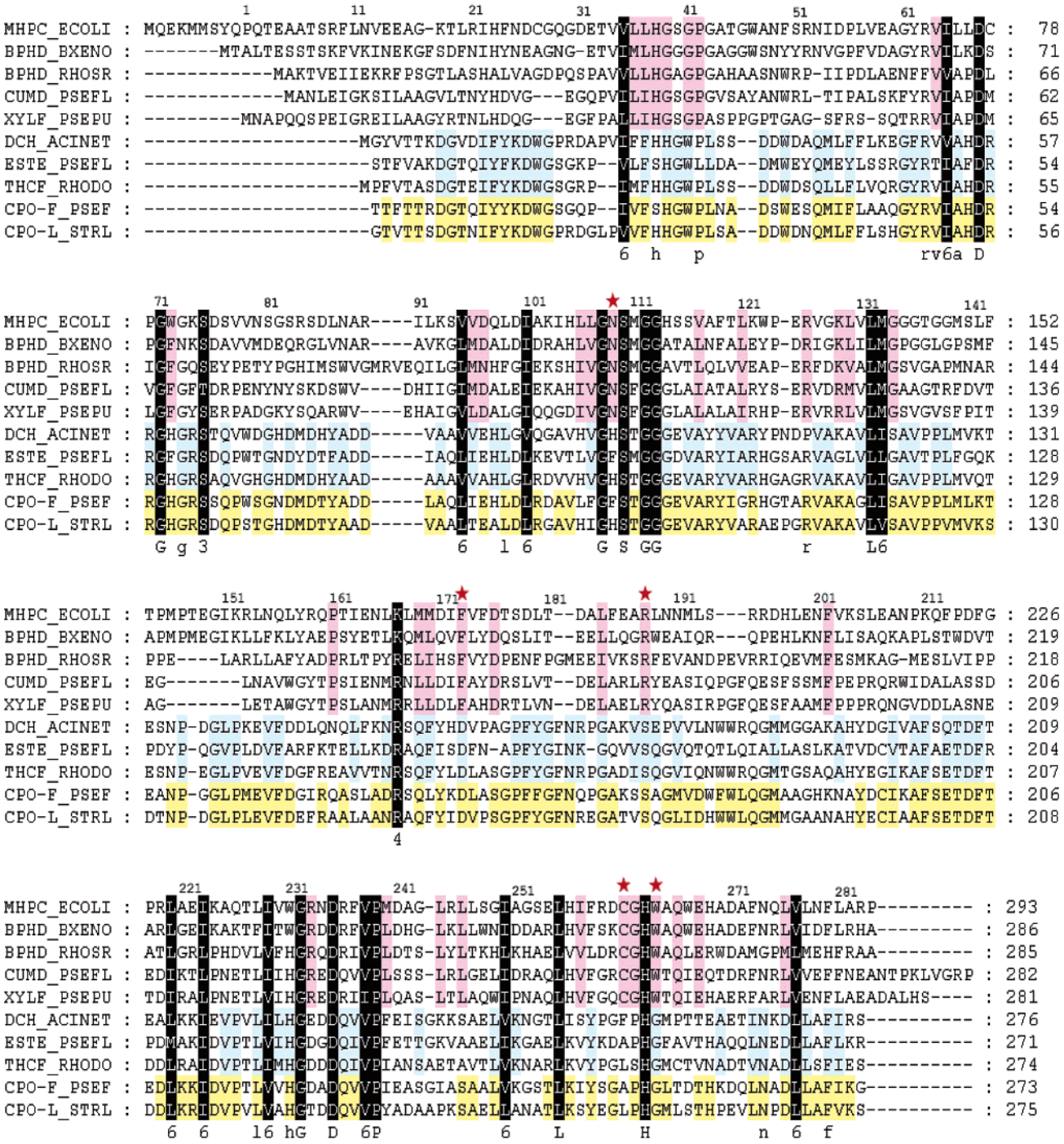

FIGURE 3: CLUSTAL W (*23*) multiple-sequence alignment of three sets of enzymes in the α/*β*-hydrolase superfamily. C−C hydrolases: (1) MhpC from *E. coli* (P77044), (2) BphD from *B. xenovorans* LB400 (YP_556398), (3) BphD from *Rhodococcus* sp. strain RHA1 (Q75WN8), (4) CumD from *Pseudomonas fluorescens* IP01 (P96965), and (5) XylF from *P. putida* (P23106). Esterases: (6) dihydrocoumarin hydrolase from *Acinetobacter calcoaceticus* (BAC55927), (7) esterase from *P. fluorescens* (P22862), and (8) ThcF esterase from *Rhodococcus erythropolis* (AAC45285). Cofactor-independent haloperoxidases: (9) CPOL from *Streptomyces lividans* (P49323) and (10) CPOF from *P. fluorescens* (031158). Completely conserved residues are colored black, and residues specifically conserved in one group are colored pink, blue, and yellow, respectively. The residues investigated in this paper are denoted with red stars. The numbering scheme is based on that of *E. coli* MhpC (*13*).

side chain of Trp-264, which is adjacent to His-263 of the catalytic triad. The side chain of Asn-109 is positioned quite close to the catalytic Ser-110, 3.5 Å from the bound substrate. Although the side chain of Cys-261 points away from the active site in the MhpC structure (*15*), the inactivation of MhpC by *p*-hydroxymercuribenzoate (*9*) suggested that this residue might be required for catalysis. These five residues were selected for site-directed mutagenesis.

Construction of Site-Directed Mutants of MhpC and BphD. Site-directed mutants were constructed from the *E. coli mhpC* and *B. xenovorans* LB400 *bphD* genes, using Quikchange site-directed mutagenesis kits (Stratagene) and overlap extension PCR-based methods. For *E. coli* MhpC, Arg-188 was replaced with Gln and Lys, Phe-173 was replaced with Gly, Asn-109 was replaced with Ala and His, and Trp-264 was replaced with Gly. For BphD, Arg-190 was replaced with

Table 2: Steady-State Kinetic Parameters for MhpC and BphD Mutant Enzymes[a]

variant	K_M (μM)	k_{cat} (s^{-1})	k_{cat}/K_M (M^{-1} s^{-1})
wild-type MhpC[b]	6.8	28	4.1×10^6
N109A	4.0	0.13	3.3×10^4
N109H	4.0	0.08	1.9×10^4
F173G	58	7.5	1.3×10^5
F173D	10	0.26	2.6×10^4
R188Q	77	0.10	1.4×10^3
R188K	38	0.74	1.9×10^4
C261A	4.2	12	2.9×10^6
W264G	125	2.7	2.1×10^4
wild-type BphD[c]	2.0	6.5	3.3×10^6
R188Q	28.2	0.016	5.7×10^2
R188K	2.0	0.009	2.8×10^3

[a] K_M and k_{cat} of MhpC and BphD mutants were determined in 50 mM phosphate buffer (pH 8.0) at 25 °C, using corresponding natural substrates. The error is ±10%. [b] Data from ref *15*. [c] Data from ref *29*.

Gln and Lys. MhpC mutants were expressed and purified to >95% purity with an ion exchange column. BphD mutants were expressed as N-terminal His_6 fusion proteins and purified to homogeneity by affinity chromatography.

Steady-State Kinetic Analysis. The C−C hydrolase activity of each mutant was determined by UV−visible spectrophotometry, observing the disappearance of the dienol substrate in 50 mM potassium phosphate buffer (pH 8.0) at either 394 nm (MhpC substrate) or 434 nm (BphD substrate). Michaelis−Menten steady-state kinetic behavior was observed, and K_M and k_{cat} kinetic parameters were determined and are listed in Table 2.

Compared to the kinetic parameters for wild-type MhpC, increased K_M values were observed for the F173G (8-fold increase), R188Q (11-fold increase), and W264G (16-fold increase) mutants, consistent with roles in substrate binding. A large decrease in k_{cat} was observed for the R188Q mutant, a 300-fold decrease compared to that of the wild-type enzyme, whereas much smaller changes in k_{cat} were observed for mutants F173G (3.5-fold decrease) and W264G (10-fold decrease). This large effect on k_{cat} prompted us also to construct the R188K mutant, which exhibited a 35-fold decrease in k_{cat} and a 5-fold increase in K_m, compared with those of the wild-type enzyme. Mutants N109A and N109H exhibited 200- and 350-fold reduced k_{cat} values compared with that of the wild-type enzyme and similar K_M values. Only a 2-fold decrease in k_{cat}/K_M was observed for the C261A mutant, implying that Cys-261 is not involved in catalysis.

The steady-state kinetic parameters for the BphD mutants are also listed in Table 2. The R190Q mutant has a 400-fold reduced k_{cat}, compared with that of the wild-type enzyme, and a 14-fold increased K_M. The R190K mutant has a k_{cat} reduced 700-fold compared to that of the wild-type enzyme and a K_M similar to that of the wild-type enzyme.

Pre-Steady-State Kinetic Analysis. To study in detail the effects of replacement of Arg-188 with Gln, the pre-steady-state kinetic behavior of this mutant enzyme was studied in potassium phosphate buffer (pH 7.0), elucidating the disappearance of substrate at 394 nm (dienolate form) and 317 nm (dienol form) and the appearance of product at 270 nm.

Table 3: Pre-Steady-State Kinetic Parameters for MhpC and BphD Mutant Enzymes[a]

Wild-Type (WT) MhpC and Mutants						
	A_1 ($\times 10^3$)	k_1 (s^{-1})	A_2 ($\times 10^3$)	k_2 (s^{-1})	A_3 ($\times 10^3$)	k_3 (s^{-1})
at 394 nm						
WT	61.9 ± 0.2	148 ± 1				
R188Q	−8.5 ± 0.2	590 ± 30	−6.9 ± 0.1	37 ± 1	137 ± 1	0.031 ± 0.001
R188K	−6.8 ± 0.7	190 ± 40	−7.6 ± 0.5	27 ± 2	130 ± 14	0.410 ± 0.006
N109A	3.7 ± 0.6	56 ± 9	−13.1 ± 0.3	34 ± 1	51.4 ± 0.4	0.044 ± 0.001
at 317 nm						
WT	145.6 ± 0.2	153.2 ± 0.4				
R188Q	9.1 ± 0.3	450 ± 26	−14.0 ± 0.1	32.0 ± 0.7	306 ± 1	0.029 ± 0.001
R188K	6.5 ± 0.5	102 ± 12	−25.9 ± 0.4	34.0 ± 0.4	187 ± 2	0.404 ± 0.002
N109A	10.5 ± 0.7	63 ± 4	−14.7 ± 0.7	33 ± 1	98.9 ± 0.1	0.051 ± 0.001
at 270 nm						
WT	−131 ± 1	144 ± 2	−117 ± 1	18 ± 1		
R188Q	−461 ± 6	0.026 ± 0.001				
R188K	−192 ± 1	0.376 ± 0.002				
N109A	−201 ± 1	0.042 ± 0.001				

Wild-Type (WT) BphD and Mutants						
	A_1 ($\times 10^3$)	k_1 (s^{-1})	A_2 ($\times 10^3$)	k_2 (s^{-1})	A_3 ($\times 10^3$)	k_3 ($\times 10^3$ s^{-1})
at 434 nm						
WT	32.2 ± 0.4	220 ± 6	65.5 ± 0.3	21.3 ± 0.1		
R188Q	101.5 ± 0.4	0.090 ± 0.001	62.7 ± 0.2	0.007 ± 0.0001		
R188K	−23.7 ± 0.1	31.3 ± 0.5	179 ± 1	1.40 ± 0.02	22.4 ± 0.5	1.0 ± 0.1
at 341 nm						
WT	20.0 ± 0.6	340 ± 10	9.1 ± 0.1	14.7 ± 0.3		
R188Q	7.7 ± 0.3	0.20 ± 0.01	12.0 ± 0.1	0.009 ± 0.0001		
R188K	36.3 ± 0.4	11.9 ± 0.3	20.5 ± 0.4	1.90 ± 0.03	0.90 ± 0.06	3.0 ± 0.5
at 270 nm[b]						
WT	−40.5 ± 0.3	32.7 ± 0.4				
R188Q	−51.3 ± 0.3	0.060 ± 0.001				
R188K	−57.2 ± 0.3	0.10 ± 0.01				

[a] Stopped-flow data were measured in 50 mM potassium phosphate (pH 7.0) at room temperature, with the enzyme and corresponding substrate mixed equivalently (1:1 [E]:[S]). Substrate consumption was monitored at 394 and 317 nm for the MhpC reaction and at 434 and 341 nm for the BphD reaction. Product appearance of both reactions was assessed at 270 nm. [b] Data recorded at 270 nm contain overlapping absorbances for HPD and benzoic acid product.

The data are given in Table 3. For wild-type MhpC (*15*), a two-step process is observed, corresponding to a fast ketonization step ($k_1 = 150$ s^{-1}), followed by rate-limiting C−C cleavage ($k_2 = 18$ s^{-1}).

The data obtained for MhpC R188Q at 317 nm could be modeled by a treble-exponential rate equation, corresponding to a three-step kinetic mechanism. The first phase, observed in the first 5 ms, resulted in an increase in A_{394} and a simultaneous decrease in A_{317}, indicating that this initial fast step corresponds to the deprotonation of the dienol substrate by the catalytic base His-263, generating the dienolate form. This behavior has been observed previously for an S40A mutant of MhpC (*15*). The second step gives an increase in A_{394} and A_{317}, with a rate constant of 32 s^{-1}. The third step gives a decrease in A_{394} and A_{317}, with a rate constant of 0.03 s^{-1}. The data observed at 270 nm could be modeled by a single-exponential equation, with a rate constant of 0.03 s^{-1}.

The observation of an intermediate step in which the substrate absorbance increases has been seen previously in the case of an S110A mutant of MhpC (*15*), in which case it was observed after a fast ketonization step, although it is not seen in the wild-type enzyme. We previously assigned this to an isomerization of the bound RFP^k intermediate to a new nonproductive ES′ species (*15*). In the case of R188Q, there is no observable initial ketonization step. Therefore, we interpret that the intermediate step is in fact due to a conformational change of the protein, which causes an increase in the extinction coefficient of the bound substrate. The third step, with a rate constant of 0.03 s^{-1}, must therefore correspond to substrate ketonization, and the subsequent C−C cleavage step must occur at a faster rate and is, therefore, not observed.

A further site-directed mutant, in which Arg-188 of MhpC is replaced with Lys, was analyzed in the same way. In this mutant, a fast initial step ($k_1 = 190$ s^{-1}) was also observed, corresponding to substrate deprotonation, followed by the step showing an increase in absorbance ($k_2 = 27$ s^{-1}), followed by a slow catalytic step ($k_3 = 0.41$ s^{-1}), which we identify as substrate ketonization. Therefore, the R188K mutant also exhibits rate-limiting substrate ketonization, though ketonization is 10-fold faster than for the R188Q mutant.

The corresponding residue in *B. xenovorans* BphD, Arg-190, was also replaced with Gln and Lys. Pre-steady-state kinetic data collected for the R190Q BphD mutant could be modeled by a two-step kinetic mechanism, corresponding to a slow initial ketonization step ($k_1 = 0.09$ s^{-1}), and rate-limiting C−C cleavage ($k_2 = 0.007$ s^{-1}). Pre-steady-state kinetic data for the R190K mutant could be modeled by a three-step kinetic mechanism, corresponding to an initial substrate deprotonation step ($k_1 = 31$ s^{-1}), followed by ketonization ($k_2 = 1.4$ s^{-1}) and C−C cleavage ($k_3 = 1.0$ s^{-1}) steps. Compared with the MhpC mutants, a similar, large effect is seen on the substrate ketonization step upon replacement of Arg-190, although in this enzyme C−C cleavage is rate-limiting, and the Lys mutant is 15-fold faster for substrate ketonization.

Pre-steady-state kinetic analysis was also carried out on MhpC mutant N109A. For this mutant, the initial ketonization step ($k_1 = 56$ s^{-1}) is reduced 3-fold compared with that of the wild-type enzyme, followed by the "increase step" seen above ($k_2 = 34$ s^{-1}), followed by a slow, rate-limiting C−C cleavage step ($k_3 = 0.044$ s^{-1}), 400-fold slower than that of the wild-type enzyme. These effects are comparable to those observed previously for mutant S110A (*15*), implying that Asn-109 is important for positioning the loop containing Ser-110.

Table 4: Diffraction Data and Statistics for MhpC H263A−Succinate Structure Determination

diffraction data	
beamline	ESRF ID23.1
wavelength (Å)	1.069
space group	$P4_32_12$
unit cell parameters (Å)	$a = b = 80.295$, $c = 427.038$
resolution (Å)	33−2.00 (2.11−2.00)
no. of measurements	999969
no. of unique reflections	83966
completeness (%)	88.1 (53.6)
R_{merge}	0.102 (0.372)
$\langle I\rangle/\langle\sigma(I)\rangle$	19.6 (4.6)
refinement statistics	
resolution range (Å)	25−2.00
R_{cryst} (%)	19.5
R_{free} (%)	22.9
rms deviations	
bonds (Å)	0.0054
angles (deg)	1.1804
average B factor (Å^2)	
protein	25.7
succinate	35.5
Ramachandran plot	
most favored regions (%)	93.5
additionally favored regions (%)	5.8

Structure Analysis of H263A MhpC. Cocrystallisation of succinate, the product of the MhpC reaction, with mutant H263A gave crystals diffracting to 2.0 Å. This complex is one of a range of structure investigations seeking to image the entire reaction path of the enzyme. It is presented here because it shows clear conformational changes of residues in the active site that are unique to the C−C hydrolases. Data collection and processing statistics are included in Table 4. Molecular replacement revealed four molecules in the asymmetric unit, organized as two 16-β-strand dimers as described previously. Structure refinement statistics are included in Table 4.

The overall structure of the mutant enzyme was very similar to that reported for the native enzyme (*13*); however, the asymmetry of the enzyme dimer was more pronounced than for the native enzyme. The succinate ligand was bound to the active site, interacting with His-114 and Ser-110 at the P end of the substrate channel. The occupancy of the succinate was clearly variable, with strong density in some protomers and weaker density in others.

Succinate occupation was correlated with altered positions for the side chains of Phe-173 and Trp-264. In the native enzyme, the ring plane of Phe-173 is orthogonal to those of the adjacent Phe-237 and Trp-264 residues such that the edges of the Phe-173 ring pack against these rings (see Figure 4). In this arrangement, Trp-264 stacks with Trp-267. This side chain can adopt two coplanar orientations related by a 180° rotation about the $C_\alpha-C_\beta$ bond, offering equivalent interactions with Trp-264. In subunit B of the mutant enzyme structure, where little succinate is bound, the arrangement of these aromatic residues is like that of the native enzyme. However, in subunit C, which interacts with B to define the active enzyme dimer, there is strong succinate density and

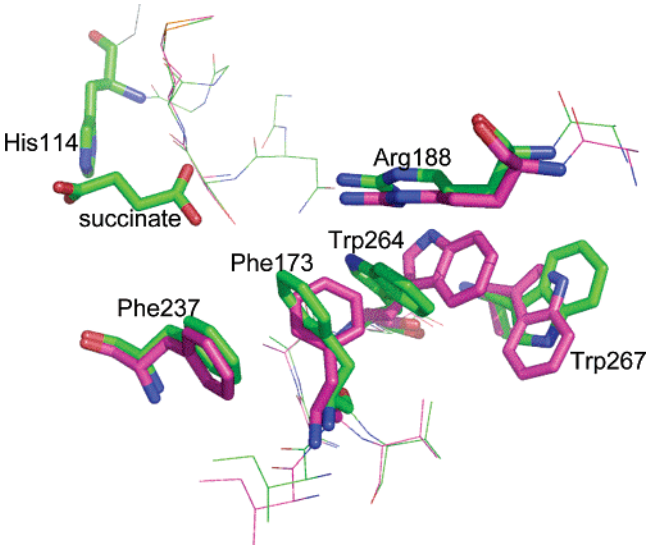

FIGURE 4: Structure of the H263A MhpC−succinate complex, showing the two observed conformations for Phe-173 and Trp-264.

the network of aromatic side chains is altered. The side chain ring plane of Phe-173 has rotated by approximately 90° to become coplanar and stacked against Phe-237. At the same time, the Trp-264 side chain has moved to stack against the other face of the Phe-173 ring and given up its previous stacking interaction with Trp-267.

These adjustments produce a stable three-layer aromatic stack, positioned close to Arg-188, and adjacent to the approach path for substrate toward Arg-188, and would therefore be expected to have an influence on substrate binding. In subunits A and D, the succinate site appears to be partially occupied and Phe-173 and Trp-263 are present with both of the conformations seen for subunits B and C and partial occupancy. The alternate conformations for these large aromatic side chains show prominent difference map peaks, which clearly show how the different arrangements can be modeled by simple bond rotations.

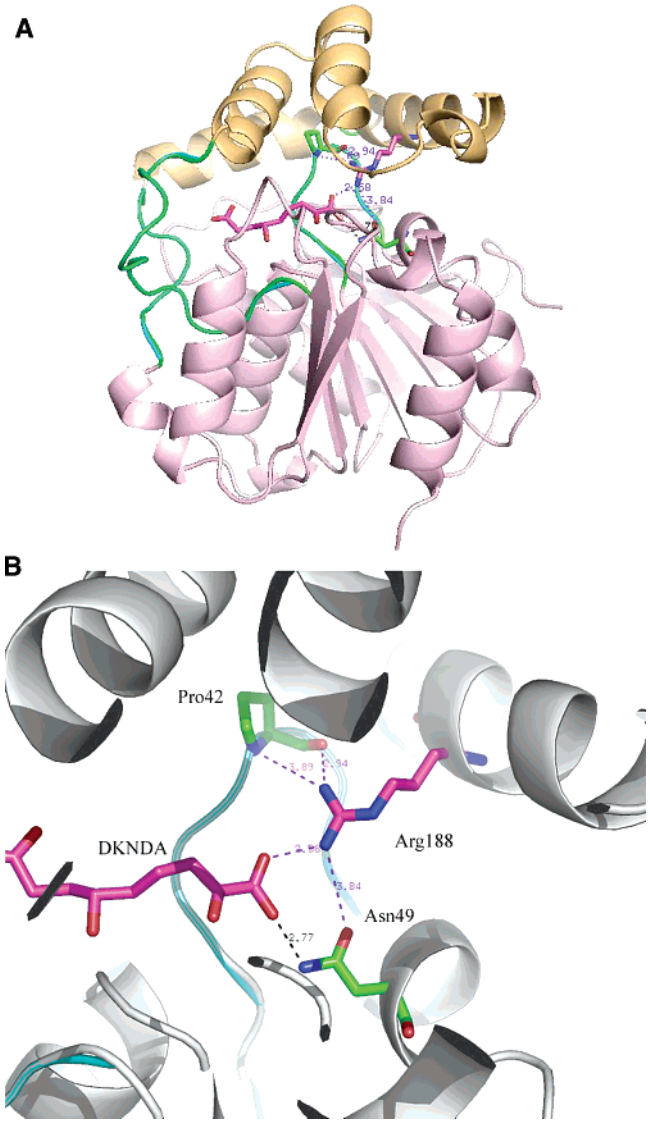

FIGURE 5: (A) Structure of the MhpC−DKNDA complex, showing the lid domain, the hinge region, and the location of Arg-188. (B) Close-up of the active site, showing the hydrogen bond network around the C-1 carboxylate involving the side chain of Arg-188.

DISCUSSION

The existence of "superfamilies" of enzymes of related structure but different function is an intriguing topic in structural biology. The haloperoxidase family of α/β-hydrolases includes enzymes possessing a variety of functions: esterases and lipases, C−C hydrolases, cofactor-independent haloperoxidases, peptidases, acyl thioesterases, cofactor-independent dioxygenases, and two enzymes bearing an aspartic acid nucleophile, haloalkane dehalogenase and epoxide hydrolase (*24*). To investigate which factors might be responsible for C−C hydrolase activity in particular, we have identified five residues that are conserved in sequences of bacterial C−C hydrolases, but not found in other enzymes of this family.

Replacement of Phe-173 and Trp-264 with Gly causes 8- and 16-fold increases, respectively, in K_M, with modest reductions in k_{cat}, implying that these residues are primarily involved in substrate binding. They are positioned close to the diene portion of the substrate; therefore, it is reasonable to propose that favorable hydrophobic and $\pi-\pi$ interactions could be formed between the dienol substrate and these residues, which would provide some specificity for these dienol substrates. Replacement of Cys-261 with Ala causes only a small decrease in k_{cat}/K_M, implying that it is not involved in catalysis; the inactivation of MhpC by *p*-mercuribenzoate (but not iodoacetate) may be caused by blocking access to the active site (*9*). Replacement of Asn-109 with Ala or His causes 200−300-fold reductions in k_{cat} and effects upon pre-steady-state kinetics similar to that observed previously for an S110A mutant (*15*). Since the side chain of Asn-109 is positioned >5 Å from the C-6 carbonyl of DKNDA in the MhpC complex (see Figure 2), it is unlikely that it is involved in oxyanion stabilization but probable that it is important in positioning the loop containing Ser-110.

The side chain of Arg-188 is positioned close to the C-1 carboxylate of the substrate; therefore, one would expect this residue to be involved primarily in substrate binding, through electrostatic and hydrogen bonding interactions. However, replacement of Arg-188 with Gln caused a remarkable 300-fold reduction in k_{cat}, which implies that this residue has some catalytic role. To investigate whether the presence of a charged side chain is important, we have also constructed

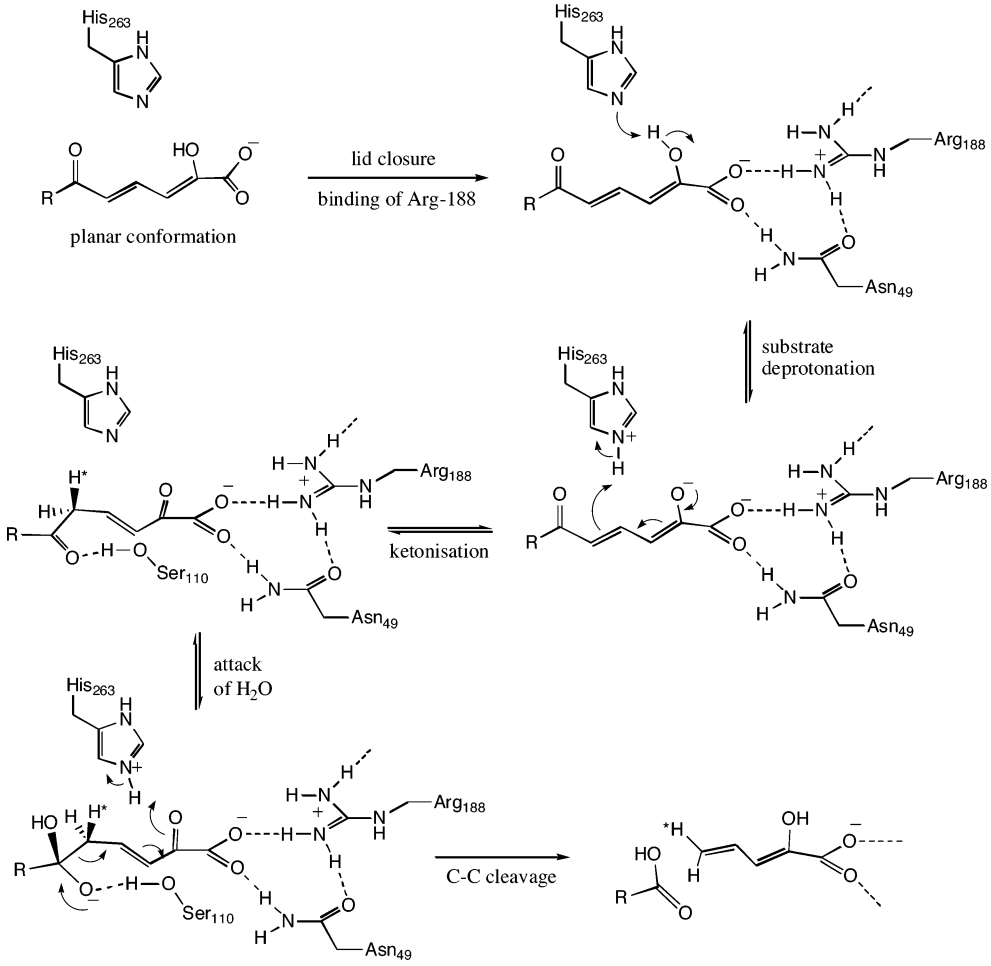

FIGURE 6: Proposed mechanism for substrate ketonization and C−C cleavage, illustrating the role of Arg-188.

the R188K mutant, which also shows a substantial reduction (35-fold) in k_{cat}, implying that the presence of the guanidinium side chain of Arg-188 is of particular importance. The catalytic function of Arg-188 is, however, not immediately obvious, since it is located far from Ser-110, and >5 Å from C-2 of DKNDA in the MhpC complex (see Figure 2); therefore, it cannot be directly involved in transition-state stabilization.

The pre-steady-state kinetic analysis of the R188Q MhpC mutant reveals a three-step kinetic mechanism: a very fast (450 s^{-1}) substrate deprotonation, followed by a step leading to an increased extinction coefficient (32 s^{-1}), which we interpret as a protein conformational change, and finally a slow catalytic step (0.03 s^{-1}) whose magnitude matches the rate of product formation at 270 nm. In previous site-directed mutants, we have been able to observe two catalytic steps, corresponding to substrate ketonization and C−C cleavage (*15*). In this case, therefore, it appears that substrate ketonization has become rate-limiting and that the subsequent C−C cleavage is faster and is therefore not observable. Evidently, the presence of Arg-188 is essential for the rapid ketonization of the substrate.

Two experimental observations suggest that a conformational change occurs in the catalytic cycle. Pre-steady-state kinetic analysis has shown a step of rate ∼30 s^{-1} which results in an increased absorbance of the bound substrate, in mutants S110A, N109A, and R188Q of MhpC. It is known from studies of proteins such as bacteriorhodopsin (*25*) and *β*-crustacyanin (*26*), which bind carotenoid chromophores, that changes in substrate conformation or the formation of protein−ligand interactions can dramatically alter the chromophore absorbance. The second observation is the mobility of Phe-173 and Trp-264 in the structure of the H263A−succinate complex. Arg-188 and Phe-173 are both part of the lid domain which is connected via a hinge region (see Figure 5A) and which must open and close over the active site during the catalytic cycle.

Close examination of the MhpC−DKNDA structure also reveals that there is a hydrogen bond network around the C-1 carboxylate of the bound substrate, involving the side chains of Arg-188 and Asn-49, and the backbone amide of Pro-42, as shown in Figure 5B. The presence of this H-bond network is also noted in the structure of C−C hydrolase CarC (*27*).

Our rationalization is that the hydrogen bond network is required to position the substrate for catalysis. The kinetic data imply that mutation of Arg-188 in MhpC (or Arg-190 in BphD) has a significant effect upon catalysis, and that effect is mainly upon substrate ketonization. We have previously deduced from stopped-flow kinetic data that MhpC is able to favor the formation of the ketonized reaction intermediate when bound to the enzyme active site, whereas the dienol form of the substrate is observed in solution by NMR spectroscopy (*10*). We have speculated that the enzyme active site may achieve this effect by destabilization of the bound substrate, perhaps via a twisted substrate conforma-

tion. It is known that the MhpC product 2-hydroxypentadienoic acid ketonizes rapidly and irreversibly (*28*), whereas the MhpC substrate, in which the dienol is stabilized by delocalization with the C-6 carbonyl group, is stable in the dienol form. We therefore propose that the binding of the substrate dienol in a twisted, nonplanar conformation, by Arg-188 and the hydrogen bond network, increases its reactivity toward ketonization. Correct positioning of the ketonized intermediate for C−C cleavage is also required so that the scissile C−C bond is anti-periplanar with respect to the C_3-C_4 bond (*29*).

The role of Arg-188 in substrate destabilization is unusual and different from catalytic functions that have been proposed for other enzyme active site arginine residues. Enzymes containing catalytic arginine residues involved directly in transition-state stabilization include phosphotransferases such as alkaline phosphatase (*30*), *Bacillus stearothermophilus* lactate dehydrogenase (*31*), *Bacillus subtilis* chorismate mutase (*32*), and *P. putida* 4-oxalocrotonate tautomerase (*33*). Active site arginine residues have been proposed to act as catalytic bases in several enzymes (*34*).

The data in this paper imply that Arg-188 has an essential role in C−C hydrolytic cleavage in the α/β-hydrolase superfamily, which would explain why this residue is found in the sequences of all bacterial C−C hydrolases of this family (Figure 3); the factors that control other types of reactivity in this superfamily are currently under investigation.

REFERENCES

1. Ollis, D. L., Cheah, E., Cygler, M., Dijkstra, B., Frolow, F., Franken, S. M., Harel, M., Remington, S. J., Silman, I., Schrag, J., Sussman, J. L., Verschueren, K. H. G., and Goldman, A. (1992) The α/β hydrolase fold, *Protein Eng. 5*, 197−211.
2. Heikinheimo, P., Goldman, A., Jeffries, C., and Ollis, D. L. (1999) Of barn owls and bankers: A lush variety of α/β hydrolase, *Structure 7*, R141−R146.
3. Schrag, J. D., and Cygler, M. (1997) Lipases and the α/β hydrolase fold, *Methods Enzymol. 284*, 85−107.
4. Nardini, M., and Dijkstra, B. W. (1999) α/β hydrolase fold enzymes: The family keeps growing, *Curr. Opin. Struct. Biol. 9*, 732−737.
5. Franken, S. M., Rozeboom, H. J., Kalk, K. H., and Dijkstra, B. W. (1991) Crystal structure of haloalkane dehalogenase: An enzyme to detoxify halogenated alkanes, *EMBO J. 10*, 1297−1302.
6. Nardini, M., Ridder, I. S., Rozeboom, H. J., Kalk, K. H., Rink, R., Janssen, D. B., and Dijkstra, B. W. (1999) The X-ray structure of epoxide hydrolase from *Agrobacterium radiobacter* AD1: An enzyme to detoxify harmful epoxides, *J. Biol. Chem. 274*, 14579−14586.
7. Fülöp, V., Böcskei, Z., and Polgar, L. (1998) Prolyl oligopeptidase: An unusual β-propeller domain regulates proteolysis, *Cell 94*, 161−170.
8. Diaz, E., and Timmis, K. N. (1995) Identification of functional residues in a 2-hydroxymuconic semialdehyde hydrolase: A new member of the α/β hydrolase-fold family of enzymes which cleaves carbon-carbon bonds, *J. Biol. Chem. 270*, 6403−6411.
9. Lam, W. W. Y., and Bugg, T. D. H. (1997) Purification, characterisation and stereochemical analysis of a C-C hydrolase: 2-Hydroxy-6-keto-nona-2,4-diene 1,9-dioic acid 5,6-hydrolase, *Biochemistry 36*, 12242−12251.
10. Henderson, I. M. J., and Bugg, T. D. H. (1997) Pre-steady state kinetic analysis of 2-hydroxy-6-keto-nona-2,4-diene 1,9-dioic acid 5,6-hydrolase: Kinetic evidence for enol/keto tautomerisation, *Biochemistry 36*, 12252−12258.
11. Fleming, S. M., Robertson, T. A., Langley, G. J., and Bugg, T. D. H. (2000) Catalytic mechanism of a C-C hydrolase enzyme: Evidence for a *gem*-diol intermediate, not an acyl enzyme, *Biochemistry 39*, 1522−1531.
12. Speare, D. M., Fleming, S. M., Beckett, M. N., Li, J.-J., and Bugg, T. D. H. (2004) Synthetic 6-aryl 2-hydroxy-6-keto-hexa-2,4-dienoic acid substrates for C-C hydrolase BphD: Investigation of a general base catalytic mechanism, *Org. Biomol. Chem. 2*, 2942−2950.
13. Dunn, G., Montgomery, M. G., Mohammed, F., Coker, A., Cooper, J. B., Robertson, T., Garcia, J.-L., Bugg, T. D. H., and Wood, S. P. (2005) The structure of the C-C bond hydrolase MhpC provides insights into its catalytic mechanism, *J. Mol. Biol. 346*, 253−265.
14. Speare, D. M., Fleming, S. M., Beckett, M. N., Li, J.-J., and Bugg, T. D. H. (2004) Synthetic 6-aryl-2-hydroxy-6-ketohexa-2,4-dienoic acid substrates for C-C hydrolase BphD: Investigation of a general base catalytic mechanism, *Org. Biomol. Chem. 2*, 2942−2950.
15. Li, C., Montgomery, M. G., Mohammed, F., Li, J.-J., Wood, S. P., and Bugg, T. D. H. (2005) Catalytic mechanism of C-C hydrolase MhpC: Elucidation of the roles of His-263 and Ser-110 from kinetic analysis of site-directed mutant enzymes, *J. Mol. Biol. 346*, 241−251.
16. Ho, S. N., Hunt, H. D., Horton, R. M., Pullen, J. K., and Pease, L. R. (1989) Site-directed mutagenesis by overlap extension using the polymerase chain reaction, *Gene 77*, 51−59.
17. Powell, H. R. (1999) The Rossmann Fourier autoindexing algorithm in MOSFLM, *Acta Crystallogr. D55*, 1690−1695.
18. Collaborative Computational Project, Number 4 (1994) The CCP4 Suite: Programs for Protein Crystallography, *Acta Crystallogr. D50*, 760−763.
19. Vagin, A., and Teplyakov, A. (1997) MOLREP: An automated program for molecular replacement, *J. Appl. Crystallogr. 30*, 1022−1025.
20. Brunger, A. T., Adams, P. D., Clore, G. M., DeLano, W. L., Gros, P., Grosse-Kunstleve, R. W., Jiang, J.-S., Kuszewski, J., Nilges, N., Pannu, N. S., Read, R. J., Rice, L. M., Simonson, T., and Warren, G. L. (1998) Crystallography and NMR system (CNS): A new software system for macromolecular structure determination, *Acta Crystallogr. D54*, 905−921.
21. *QUANTA96* (1996) X-ray structure analysis user's reference, Molecular Simulations, San Diego.
22. DeLano, W. L. (2002) *The PyMOL Molecular Graphics System*, DeLano Scientific, San Carlos, CA.
23. Thompson, J. D., Higgins, D. G., and Gibson, T. J. (1994) CLUSTALW: Improving the sensitivity of progressive multiple sequence alignment through sequence weighting, position-specific gap penalties and weight matrix choice, *Nucleic Acids Res. 22*, 4673−4680.
24. Bugg, T. D. H. (2004) Diverse catalytic activities in the α/β-hydrolase family: Activation of H_2O, H_2O_2, HCN, and O_2, *Bioorg. Chem. 32*, 367−375.
25. Aharoni, A., Khatchatouriants, A., Manevitch, A., Lewis, A., and Sheves, M. (2003) Protein-β-ionone ring interactions enhance the light-induced dipole of the chromophore in bacteriorhodopsin, *J. Phys. Chem. B 107*, 6221−6225.
26. Cianci, M., Rizkallah, P. J., Olczak, A., Raftery, J., Chayen, N. E., Zagalsky, P. F., and Helliwell, J. R. (2002) The molecular basis of the coloration mechanism in lobster shell: β-Crustacyanin at 3.2 Å resolution, *Proc. Natl. Acad. Sci. U.S.A. 99*, 9795−9800.
27. Habe, H., Morii, K., Fushinobu, S., Nam, J.-W., Ayabe, Y., Yoshida, T., Wakagi, T., Yamane, H., Nojiri, H., and Omori, T. (2003) Crystal structure of a histidine-tagged serine hydrolase involved in the carbazole degradation (CarC enzyme), *Biochem. Biophys. Res. Commun. 303*, 631−639.
28. Pollard, J. R., and Bugg, T. D. H. (1998) Purification, characterisation and reaction mechanism of monofunctional 2-hydroxypentadienoic acid hydratase from *Escherichia coli*, *Eur. J. Biochem. 251*, 98−106.
29. Li, J.-J., and Bugg, T. D. (2005) Stereochemistry of the reaction catalysed by 2-hydroxy-6-keto-6-phenyl-hexa-2,4-dienoic acid 5,6-hydrolase (BphD), *Chem. Commun.*, 130−132.
30. Holtz, K. M., Stec, B., and Kantrowitz, E. R. (1999) A model of the transition state in the alkaline phosphatase reaction, *J. Biol. Chem. 274*, 8351−8354.
31. Clarke, A. R., Wilks, H. M., Barstow, D. A., Atkinson, A., Chia, W. N., and Holbrook, J. J. (1988) An investigation of the contribution made by the carboxylate group of an active site

histidine-aspartate couple to binding and catalysis in lactate dehydrogenase, *Biochemistry 27*, 1617−1622.
32. Chook, Y. M., Gray, J. V., Ke, H., and Lipscomb, W. N. (1994) The monofunctional chorismate mutase from *Bacillus subtilis*: Structure determination of chorismate mutase and its complexes with a transition state analog and prephenate, and implications for the mechanism of the enzymatic reaction, *J. Mol. Biol. 240*, 476−500.
33. Azurmendi, H. F., Miller, S. G., Whitman, C. P., and Mildvan, A. S. (2005) Half-of-the-sites binding of reactive intermediates and their analogues to 4-oxalocrotonate tautomerase and induced symmetry of the enzyme, *Biochemistry 44*, 7725−7737.
34. Guillen-Sclippe, Y. V., and Hedstrom, L. (2005) A twisted base? The role of arginine in enzyme-catalyzed proton abstractions, *Arch. Biochem. Biophys. 433*, 266−278.
35. Li, J.-J., Li, C., Blindauer, C. A., and Bugg, T. D. H. (2006) Evidence for a *gem*-diol reaction intermediate in bacterial CC hydrolase enzymes BphD and MhpC from ^{13}C NMR spectroscopy, *Biochemistry 45*, pp 12461-12469.

BI061253T